Shell model for drag reduction with polymer additives in homogeneous turbulence

Roberto Benzi,[1] Elisabetta De Angelis,[2] Rama Govindarajan,[3] and Itamar Procaccia[4,5]
[1]*Dipartimento di Fisica and INFM, Università "Tor Vergata," Via della Ricerca Scientifica 1, I-00133 Roma, Italy*
[2]*Engineering Mechanics Unit, Jawaharlal Nehru Centre for Advanced Scientific Research, Jakkur, Bangalore 560064, India*
[3]*Dipartimentao di Meccanica e Aeronautica, Università di Roma La Sapienza, Via Eudossiana 18, Roma 00184, Italy*
[4]*Department of Chemical Physics, The Weizmann Institute of Science, Rehovot 76100, Israel*
[5]*Department of Physics, The Chinese University of Hong Kong, Shatin, Hong Kong*
(Received 2 March 2003; published 23 July 2003)

Recent direct numerical simulations of the finite-extensibility nonlinear elastic dumbbell model with the Peterlin approximation of non-Newtonian hydrodynamics revealed that the phenomenon of drag reduction by polymer additives exists (albeit in reduced form) also in homogeneous turbulence. We use here a simple shell model for homogeneous viscoelastic flows, which recaptures the essential observations of the full simulations. The simplicity of the shell model allows us to offer a transparent explanation of the main observations. It is shown that the mechanism for drag reduction operates mainly on large scales. Understanding the mechanism allows us to predict how the amount of drag reduction depends on the various parameters in the model. The main conclusion is that drag reduction is not a universal phenomenon; it peaks in a window of parameters such as the Reynolds number and the relaxation rate of the polymer.

DOI: 10.1103/PhysRevE.68.016308 PACS number(s): 47.27.Nz, 47.27.Ak

I. INTRODUCTION

The phenomenon of drag reduction by polymer additives is usually studied in channels or pipes, where the boundary conditions and the effects of the walls are very important [1–4]. Until recently, it was not known whether drag reduction could be achieved also in homogeneous flows; this question has been answered recently in the affirmative, via direct numerical simulations (DNS) of the finite-extensibility nonlinear elastic dumbbell model with the Peterlin approximation (FENE-P) equations [5,6] in homogeneous conditions (i.e., in a box with periodic boundary conditions) [7]. The FENE-P takes into account the effect of the polymers on the Newtonian fluid by introducing the conformation tensor $\boldsymbol{R}$ of the polymers into the fluid stress tensor [8]. The FENE-P equations are known to model well the effects of polymers on the hydrodynamic flows, and DNS of these equations in channel geometry recaptured very well the characteristics of drag reduction in experimental channel turbulence [4,9]. The observation of drag reduction in homogeneous conditions offers an opportunity to investigate the phenomenon independent of boundary layers and wall effects. Nevertheless, the FENE-P equations are relatively cumbersome to analyze without the help of DNS. The aim of this paper is to introduce a shell model of the homogeneous FENE-P equations. We will demonstrate that the shell model recaptures the main findings of the homogeneous DNS, and that these findings are understandable analytically, taking advantage of the relative simplicity of the shell model. To derive the shell model for drag reduction we make use of a formal analogy between the FENE-P equations for viscoelastic flows and magnetohydrodynamics (MHD) [10]. It had been pointed out that if we form a tensor $R_{i,j}$ from the direct product of the magnetic field B_i, i.e., $R_{i,j} \equiv B_i B_j$, then the nonlinear couplings of MHD lead to equations for the tensor $\boldsymbol{R}$ whose nonlinear terms are equivalent to those of FENE-P, up to terms that remove the dynamo effect. This analogy is revisited and exploited in Sec. II. The shell model for viscoelastic flow is introduced and discussed in Sec. III. In Sec. IV, we present numerical simulations of the shell model and demonstrate the existence of drag reduction. In Sec. V, we present the mechanism of drag reduction. This is the central section of this paper. We show that drag reduction is not a universal phenomenon. Rather, it depends on parameters such as the Reynolds number and the relaxation time of the polymer. The amount of drag reduction peaks in a window of these parameters. In Sec. VI, we demonstrate that understanding the mechanism provides us with a predictive power that we can test against numerical simulations. We conclude in Sec. VII by observing that precisely because drag reduction is not a universal phenomenon it can be manipulated by optimizing parameters.

II. THE FENE-P EQUATIONS AND THEIR RELATION TO MHD

The addition of a dilute polymer to a Newtonian fluid gives rise to an extra stress tensor $\boldsymbol{\mathcal{T}}(\boldsymbol{r},t)$ which affects the Navier-Stokes equations [5,6]

$$\frac{\partial \boldsymbol{u}}{\partial t} + (\boldsymbol{u}\cdot\boldsymbol{\nabla})\boldsymbol{u} = -\boldsymbol{\nabla} p + \nu_s \boldsymbol{\nabla}^2 \boldsymbol{u} + \boldsymbol{\nabla}\cdot\boldsymbol{\mathcal{T}},$$

$$\boldsymbol{\nabla}\cdot\boldsymbol{u} = 0. \tag{1}$$

Here, $\boldsymbol{u}(\boldsymbol{r},t)$ is the solenoidal velocity field, $p(\boldsymbol{r},t)$ is the pressure, and ν_s is the viscosity of the neat fluid. In the FENE-P, the additional stress tensor $\boldsymbol{\mathcal{T}}$ is determined by the "polymer conformation tensor" $\boldsymbol{R}$ according to

$$\boldsymbol{\mathcal{T}}(\boldsymbol{r},t) = \frac{\nu_p}{\tau}\left[\frac{f(\boldsymbol{r},t)}{\rho_0^2}\boldsymbol{R}(\boldsymbol{r},t) - \boldsymbol{1}\right]; \tag{2}$$

Here **1** is the unit tensor, ν_p is a viscosity parameter, τ is a relaxation time for the polymer conformation tensor, and ρ_0 is a parameter which in the derivation of the model stands for the rms extension of the polymers in equilibrium. The function $f(\boldsymbol{r},t)$ limits the growth of the trace of $\boldsymbol{R}$ to a maximum value ρ_{m}:

$$f(\boldsymbol{r},t)\equiv\frac{\rho_{\mathrm{m}}^2-\rho_0^2}{\rho_{\mathrm{m}}^2-R_{\gamma\gamma}(\boldsymbol{r},t)}. \tag{3}$$

The model is closed by the equation of motion for the conformation tensor which reads

$$\frac{\partial R_{\alpha\beta}}{\partial t}+(\boldsymbol{u}\cdot\boldsymbol{\nabla})R_{\alpha\beta}=\frac{\partial u_\alpha}{\partial r_\gamma}R_{\gamma\beta}+R_{\alpha\gamma}\frac{\partial u_\gamma}{\partial r_\beta}-\frac{1}{\tau}[f(\boldsymbol{r},t)R_{\alpha\beta}-\rho_0^2\delta_{\alpha\beta}]. \tag{4}$$

This model was simulated by DNS in channel flow turbulence, showing a qualitative and quantitative agreement with laboratory experiments on drag reduction. Recently, the same model has been used to understand whether or not drag reduction is observed in homogeneous and isotropic conditions [7]. In homogeneous and isotropic turbulence, drag reduction can be determined by computing the ratio

$$D=\frac{\epsilon L}{E^{3/2}}, \tag{5}$$

where E is the kinetic energy, ϵ is the total rate of energy dissipation, and L is the scale of the external forcing. The above expression of drag reduction can be easily reduced to the so called skin friction factor for turbulent channel flows. The numerical simulation of homogeneous and isotropic turbulence were performed in a cube with periodic boundary conditions. The external forcing was applied with random phase in order to ensure isotropy and homogeneity. The numerical simulations were performed for the Navier-Stokes equations and the FENE-P for the *same* external forcing. Both the total energy dissipation and the kinetic energy increased for the FENE-P as compared to the Newtonian case. A direct computation of D shows that there is a drag reduction of about 20%, i.e., roughly of the same order as what had been observed in the turbulent channel flow. Also, in homogeneous and isotropic turbulence, the Taylor microscale appeared to increase, precisely as much as the buffer layers increases in channel flows [1]. This is an interesting result because it shows us that the effect of boundary conditions is not crucial for drag reduction, at least from a physical point of view. Nevertheless, it is still difficult to understand from numerical simulations, even in the homogeneous and isotropic case, that what is the physical mechanism that is responsible for drag reduction. The increase of the Taylor microscale is certainly not enough to explain quantitatively the increase of the kinetic energy, as somehow previously suggested in the literature [1,11].

Having understood that the homogeneous simulations exhibit drag reduction, we would like to propose a mechanism for it. Rather than doing it directly with the FENE-P, we would present first a simplified model. We have already shown before that drag reduction appears in simplified models such as the Burgers equation [12]. Here, we derive a shell model for the FENE-P equations. The advantage of the shell model is that it is much more tractable analytically than the full FENE-P equations. We will present the model, demonstrate explicitly that it exhibits drag reduction in much the same way as the FENE-P equations, and finally offer a different mechanism to understand the phenomenon.

III. THE SHELL MODEL

To derive a shell model of the homogeneous FENE-P equations (without boundaries) we proceed in two steps. First, we recall a recent remark [10] that the FENE-P equations can be recaptured almost entirely by taking the conformation tensor to be a diadic direct product of a vector $\boldsymbol{B}$, i.e., $R_{ij}\equiv B_iB_j$. In terms of this vector, the equations read

$$\frac{\partial\boldsymbol{u}}{\partial t}+(\boldsymbol{u}\cdot\boldsymbol{\nabla})\boldsymbol{u}=-\boldsymbol{\nabla}p+\boldsymbol{B}\cdot(\boldsymbol{\nabla}\boldsymbol{B})+\nu_{\mathrm{s}}\boldsymbol{\nabla}^2\boldsymbol{u},$$

$$\boldsymbol{\nabla}\cdot\boldsymbol{u}=0,$$

$$\frac{\partial\boldsymbol{B}}{\partial t}+(\boldsymbol{u}\cdot\boldsymbol{\nabla})\boldsymbol{B}=-\frac{\boldsymbol{B}}{\tau}+\boldsymbol{B}\cdot(\boldsymbol{\nabla}\boldsymbol{u}),$$

$$\boldsymbol{\nabla}\cdot\boldsymbol{B}=0. \tag{6}$$

These equations are identical to the FENE-P up to the explicit appearance of the function $f(\boldsymbol{r},t)$. The learned reader of course recognizes that for $\tau\to\infty$ these equations are isomorphous to MHD. We can therefore write immediately, by inspection, a shell model for FENE-P by using the well studied shell model for the MHD [13,14], including the relaxation term for finite τ. We denote the velocity field by u and the ''polymer '' field by B. The dynamical variable of the shell model are the field at wave vector k_n, denoted, respectively, as $u_n\equiv u(k_n)$ and $B_n\equiv B(k_n)$. The shell model restricts attention to wavevectors $k_n=k_0\lambda^n$, where typically in numerical simulations $\lambda=2$.

In order to derive the shell model equation, we consider the following nonlinear operator:

$$\Phi_n(u,B)=b_1k_nu_{n+2}B_{n+1}^*-b_1k_{n-1}u_{n+1}B_{n-1}^*+c_1k_nu_{n+1}^*B_{n+2}+c_1k_{n-2}u_{n-1}B_{n-2}+b_ck_{n-1}B_{n+1}u_{n-1}^*+b_ck_{n-2}u_{n-2}B_{n-1}, \tag{7}$$

where $b_1=1-b$; $c_1=1+c$; $b_c=b+c$; and $-1\leqslant b\leqslant 0$ and $c=1+b$ are the usual parameters defined in the Sabra model.

In terms of the nonlinear operator Φ, the Sabra shell model of turbulence [15] can be written as

$$\frac{du_n}{dt}=\frac{i}{3}\Phi_n(u,u)-\nu k_n^2u_n+f_n, \tag{8}$$

where f_n is an external forcing and ν the kinematic viscosity of the model. Let us remark that the following relation can be proved:

$$i\sum_n \Phi_n(u,B)B_n^* - i\sum_n \Phi_n^*(u,B)B_n = 0. \tag{9}$$

Using the nonlinear operator Φ, it is possible to model Eqs. (6) in the framework of shell models, namely,

$$\frac{du_n}{dt} = \frac{i}{3}\Phi_n(u,u) - \frac{i}{3}\Phi_n(B,B) - \nu k_n^2 u + f_n,$$

$$\frac{dB_n}{dt} = \frac{i}{3}\Phi_n(u,B) - \frac{i}{3}\Phi_n(B,u) - \frac{1}{\tau}B_n. \tag{10}$$

Equation (9) shows us that the generalized energy E,

$$E = E_u + E_B,$$

$$E_u \equiv \sum_n u_n u_n^*, \quad E_B \equiv \sum_n B_n B_n^* \tag{11}$$

is conserved in the inviscid limit, i.e., for $\tau \to \infty$ and $\nu \to 0$.

We will refer to this model as the Sabra-P model. Besides the generalized energy E, the model conserves the ''cross helicity'' in the inviscid limit

$$K = \sum_n \mathrm{Re}(u_n^* B_n). \tag{12}$$

In MHD one needs to worry about the existence of a dynamo effect, i.e., an unbounded increase in the magnetic field. In our case, the term that models the polymer relaxation time $-B_n/\tau$ will be responsible for guaranteeing stationary statistics without dynamo. In addition to the conservation laws, the equations of motion remain invariant to the phase transformations $u_n \to u_n \exp(i\phi_n)$ and $B_n \to B_n \exp(i\psi_n)$. The conditions are

$$\phi_n + \phi_{n+1} - \phi_{n+2} = 0, \tag{13}$$

$$\phi_n + \psi_{n+1} - \psi_{n+2} = 0, \tag{14}$$

$$\psi_n + \phi_{n+1} - \psi_{n+2} = 0, \tag{15}$$

$$\psi_n + \psi_{n+1} - \phi_{n+2} = 0. \tag{16}$$

This implies $\psi_n = \phi_n \ \forall \ n$. As a result of the phase constraints, there exist in this model only few nonzero correlation functions. The only second-order quantities are $\langle |u_n|^2 \rangle$ and $\langle |B_n|^2 \rangle$. The only third-order quanitites are of the form $\mathrm{Im}\langle \beta_{n-1}\beta_n\beta_{n+1}^* \rangle$, where β can be u or B.

IV. NUMERICAL INVESTIGATION OF THE SHELL MODEL: DRAG REDUCTION

In this section we compare the solutions of the shell model (10) to the usual Sabra shell model for the corresponding Newtonian flow. The Sabra model (8) is obtained from Eqs. (10) in the limit $\tau \to 0$. Alternatively, we can get the Sabra dynamics by simply taking as initial conditions $B_n = 0$.

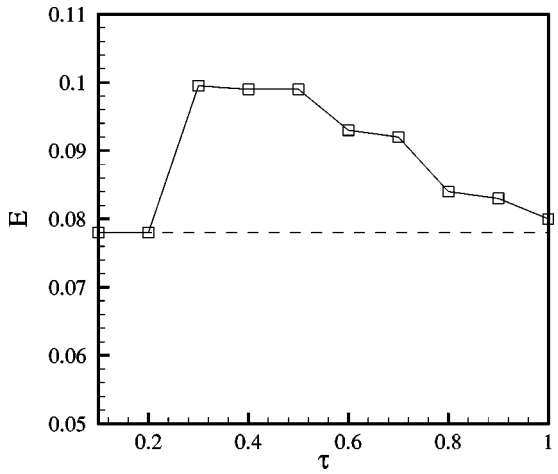

FIG. 1. Kinetic energy of the Sabra-P model for $\nu = 10^{-5}$ as a function of τ. The constant reference line corresponds to the kinetic energy computed for the Sabra model without polymer.

To have a meaningful comparison we always drive the two models with a constant power input. In other words, we choose

$$f_1 = \frac{F_a}{u_1^*}, \quad f_2 = \frac{F_b}{u_2^*}, \quad f_n = 0 \text{ for } n \geqslant 2, \tag{17}$$

with $F_a = F_b = 10^{-3}(2+2i)$. Since the power input is the same, drag reduction is exhibited in Eqs. (10) if the kinetic energy of the flow increases. The latter is simply $\langle E_u \rangle$. We will investigate the existence of drag reduction, its dependence on parameters, the question of the dissipative scale, and the dynamical signatures of drag reduction.

A. Drag reduction and its dependence on parameters

We have numerically investigated the behavior of the Sabra-P model for different values of τ and ν. In Figs. 1–3 we show $\langle E_u \rangle$ for three values of viscosity and for different values of τ. For concreteness, we have fixed the model parameter b as -0.4 in all the simulations. In all the figures, the constant line corresponds to the value of the kinetic energy computed for the Sabra model without coupling to B_n. By inspecting the three figures, one can safely state that the Sabra-P model shows drag reduction. In particular, for all cases, there is an optimal choice of τ for which the effect of drag reduction is maximal. For $\tau \to 0$ and $\tau \to \infty$, drag reduction decreases and eventually we enter a region of parameters where we observe drag enhancement. Moreover, for fixed value of τ and decreasing values of ν, drag reduction decreases, reaching a mere few percent for $\nu = 10^{-8}$.

B. Which scales are responsible for drag reduction?

To understand that which scales are responsible for the drag reduction, we compare $\langle |u_n|^2 \rangle$ for both models with ν

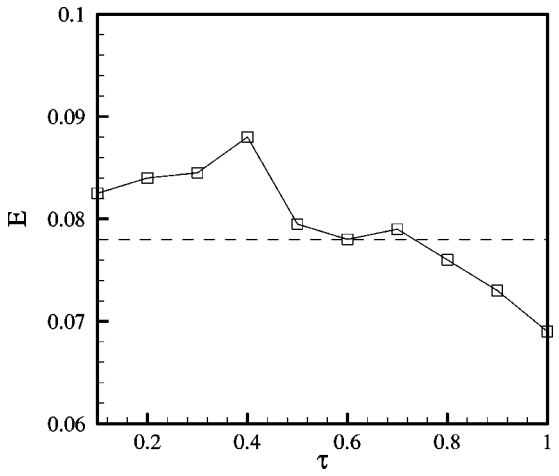

FIG. 2. Kinetic energy of the Sabra-P model for $\nu=10^{-6}$ as a function of τ. The constant reference line corresponds to the kinetic energy computed for the Sabra model without polymer.

$=10^{-5}$, again at the same power input. This is shown in Fig. 4. This figure shows us an interesting and important point. It is clear that the drag reduction is due to the relative increase in $\langle|u_n|^2\rangle$ *for small values of* n, and that this occurs at the expense of a relative decrease in $\langle|u_n|^2\rangle$ for high values of n. This finding is in close correspondence with similar conclusions obtained for the FENE-P, both in homogeneous and channel flows [16].

C. The dissipative scale

In some theories of drag reduction, it was proposed that the dissipative scale is increased in the viscoelastic flow, and that somehow this is responsible for the phenomenon [1,11,17]. To test this possibility we plot in Fig. 5 the quantity $\langle k_n^2|u_n|^2\rangle$ as a function of n. This quantity peaks at the dissipative scale, i.e., the Kolmogorov scale. Inspecting Fig. 5 shows us that the dissipative scale has not changed at all

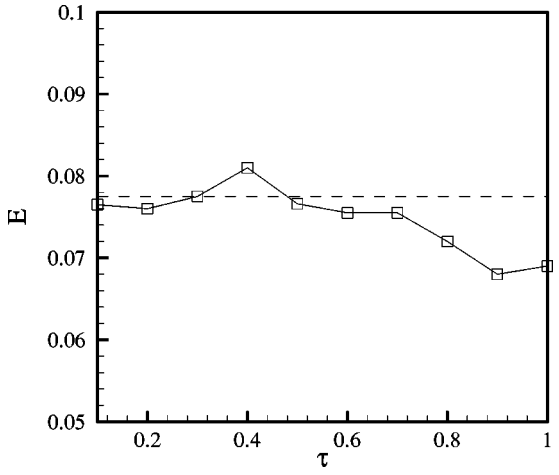

FIG. 3. Kinetic energy of the Sabra-P model with polymer for $\nu=10^{-8}$ as a function of τ. The constant reference line corresponds to the kinetic energy computed for the Sabra model without polymer.

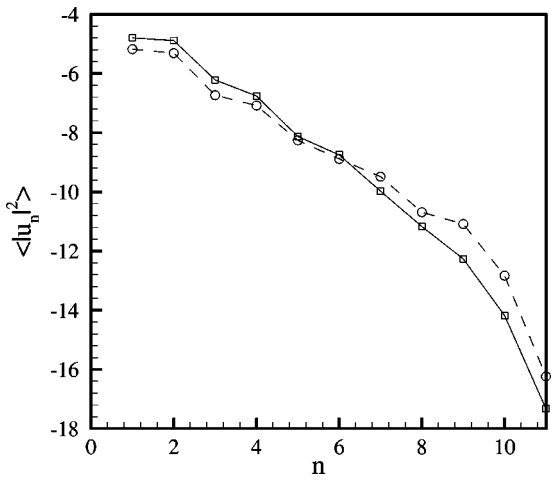

FIG. 4. A double logarithmic (to base 2) comparison of the average energy shell by shell for the Sabra (dotted line with circles) and the Sabra-P (continuous line with squares) models. Drag reduction seen is the relative increase in energy for small values of n on the expense of large values of n.

between the Sabra and the Sabra-P models, even though the latter certainly exhibits drag reduction. Thus, as indicated before, drag reduction should be understood as a phenomenon of the energy containing scales rather than the dissipative scales.

D. Dynamical signature of drag reduction

The similarity between the FENE-P and its shell analog transcends statistical quantities. To observe the close dynamical similarity it is instructive to consider the quantity

$$\Pi = i\Sigma_n u_n^* \Phi_n(B,B) - i\Sigma_n u_n \Phi_n^*(B,B), \tag{18}$$

which describes the exchange between the kinetic energy E_u and the polymer or elastic energy E_B. In Fig. 6 we show a time series of Π for $\nu=10^{-5}$. Π is always negative; the

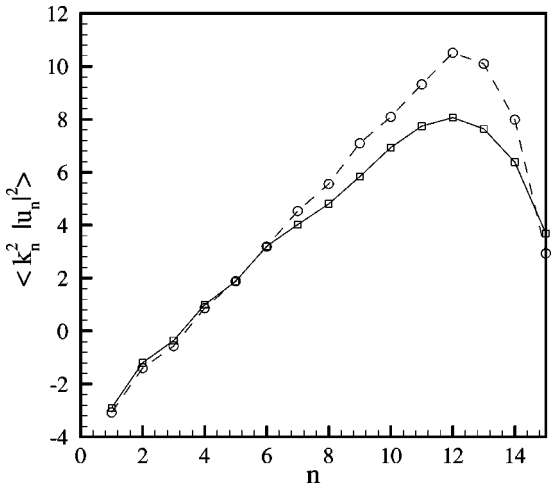

FIG. 5. Energy dissipation displayed in double logaritmic plot for each shell for the Sabra model (dotted line with circles) and for the Sabra-P model (continuous line with squares).

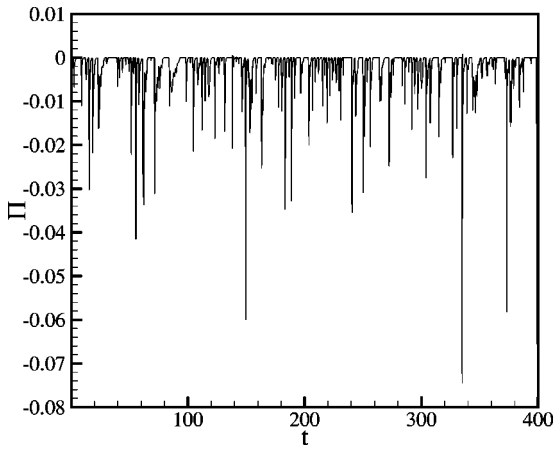

FIG. 6. Time behavior of the quantity Π as defined in the text.

effect of the polymers is to drain energy from the kinetic energy. Moreover, the dynamics of Π is strongly intermittent, which is a feature already observed in the DNS of the FENE-P. The numerical simulations indicate the conclusion that the model used in this paper shows drag reduction in a way qualitatively close to the observed behavior of the FENE-P [9].

We note in passing that it is not the first time that shell models seem to reproduce many of the features of turbulent flows; it is gratifying however that we can present a similar success even when we include relatively nontrivial effects induced by polymer dynamics.

V. MECHANISM FOR DRAG REDUCTION

This is the central section of this paper, in which we propose a detailed mechanism for drag reduction in the present model. We begin by analyzing the necessary conditions for drag reduction.

A. Necessary condition for drag reduction

To derive a necessary condition for drag reduction, let us consider the equation for the total energy, which reads

$$dE/dt=\sum_n \left[\frac{1}{2}(f_n u_n^*+f_n^* u_n)-\nu k_n^2 u_n u_n^*-\frac{1}{\tau}B_n B_n^*\right]. \tag{19}$$

At steady state, with power input maintained constant at P, we have

$$P=\Sigma_n\left[\nu k_n^2 u_n u_n^*+\frac{1}{\tau}B_n B_n^*\right]. \tag{20}$$

All the terms on the right-hand side (RHS) are strictly positive. Since the energy input P is constant for the Sabra and the Sabra-P (SP) models, we get

$$\Sigma_n k_n^2[(u_n u_n^*)_S-(u_n u_n^*)_{SP}]>0. \tag{21}$$

On the other hand, if the SP model is to be drag reducing, we must have

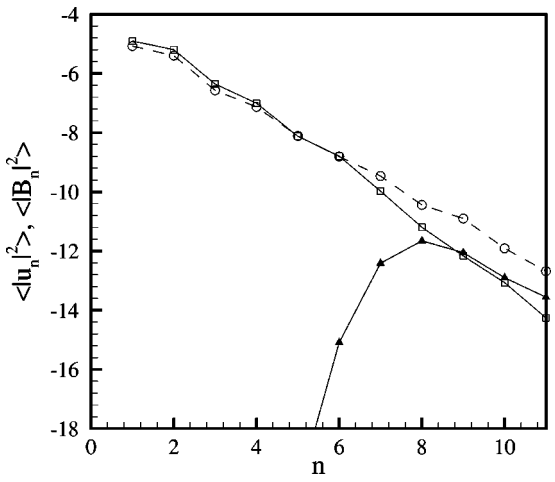

FIG. 7. Double logarithmic plot (to base 2) of the energy spectrum of the Sabra-P model (continuous line with squares) and the Sabra model (continuous line with circles) for $\nu=10^{-6}$. The continuous line with black triangles represents the energy spectrum of the B field.

$$\Sigma_n[(u_n u_n^*)_S-(u_n u_n^*)_{SP}]<0. \tag{22}$$

The only way Eqs. (21) and (22) can hold simultaneously is if for small k_n, $|u_n|_{SP}>|u_n|_S$, and sufficiently larger to compensate for the fact that at large k_n, $|u_n|_{SP}<|u_n|_S$. This means that the kinetic energy plotted versus k has to display an increased slope *at least somewhere* for drag reduction to take place. We have seen this already in Fig. 4. We show this important phenomenon once more in a log-log plot in Fig. 7, in which also the B_n-spectrum is shown for future reference. We see very clearly the crossing that occurs between the u_n spectrum of the Sabra-P model and the Sabra counterpart, which is the necessary condition for drag reduction. Note that the increase in slope is a necessary but not a sufficient condition for drag reduction. We may increase the slope but not enough to cross the Sabra spectrum, or cross but not far enough to compensate for the reduced kinetic energy at large k.

B. Typical scales related to the polymer

A discussion of the mechanism of drag reduction calls for pointing out the existence of two typical scales that were already introduced in the past in the literature on drag reduction. The first is the Lumley scale k_c, which is defined by the relaxation time of the polymer being of the same order as the eddy turnover time. For our model this scale satisfies

$$u(k_c)k_c\sim\tau^{-1}. \tag{23}$$

Note that by definition this scale is Reynolds number independent.

The other scale, which we refer to as the de Gennes scale k_g, is where the kinetic energy on the scale k_g is of the same order as the elastic energy:

$$u^2(k_g)\sim B^2(k_g). \tag{24}$$

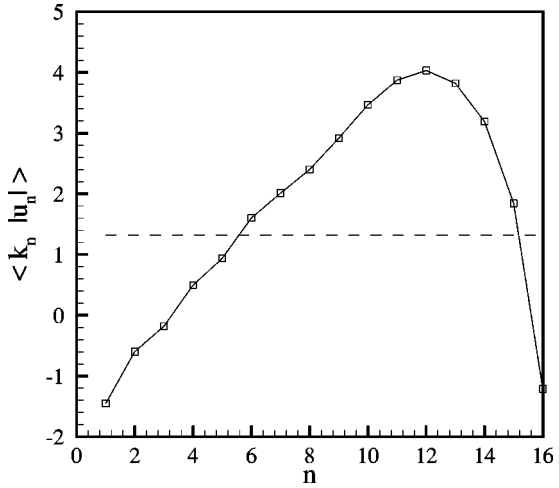

FIG. 8. Double logarithmic plot (to base 2) of the inverse of the "eddy turnover time" $\sqrt{\langle E_n \rangle} k_n$ as a function of k_n (continuous line with squares). The constant reference dotted line is τ^{-1}. The crossing in inertial range identified k_c. In this figure, $\nu = 10^{-5}$, $\tau = 0.4$.

In fact, in the Sabra-P model the scales so defined appear to be very close, if not identical to each other. In particular, we will show presently that also k_g is Reynolds number independent. To demonstrate the equivalence of the two scales we first exhibit in Fig. 8 the numerical estimate of k_c. The physical significance of k_c is not in the accidental identity of the two time scales, but rather that for k vectors smaller than k_c the effect of the B_n field on the energy flux is negligible, but not so for k vectors larger than k_c. To see this, introduce the quantities related to the energy flux in the Sabra-P model, namely,

$$S_n = \langle \mathrm{Im}(u_{n-1}^* u_n^* u_{n+1}) \rangle, \tag{25}$$

$$T_n = \langle \mathrm{Im}(B_{n-1}^* u_n^* B_{n+1}) \rangle. \tag{26}$$

The physical meaning of the two quantities is rather clear: $k_n S_n$ is proportional to the flux of the kinetic energy from large scale to small scales due to nonlinear terms, while $k_n T_n$ is proportional to the flux of kinetic energy to the polymer field. We expect that for k_n near k_c, the effect of T_n cannot be neglected in the dynamics, i.e., the average energy flux for the velocity field

$$k_n G_n = k_n (S_n - T_n) \tag{27}$$

begins to change with respect to what it is observed in the Sabra model.

In Fig. 9 we show the quantity G_n computed for the same model parameters of Fig. 8. The symbols refer to the Sabra model, while the continuous line corresponds to the Sabra-P model. In the vicinity of $n_c \sim 5.5$, the two models show a different behavior and, in particular, the Sabra-P model shows a decrease of the total energy flux $k_n G_n$, as previously claimed.

Regarding the scale k_g, it can be read from the spectrum shown in Fig. 7, in which $\nu = 10^{-6}$. In Fig. 10 we show the analogous spectra for $\nu = 10^{-8}$. Clearly, k_g did not change at

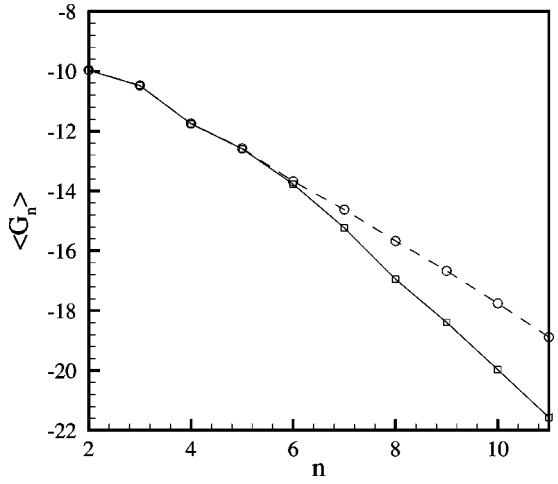

FIG. 9. Double logarithmic plot (to base 2) of G_n computed for the Sabra-P model (continuous line with squares) and the Sabra model (dotted lines with circles).

all, in agreement with our assertion that it is Reynolds independent. Finally, we note that in all the figures shown, k_c and k_g are of the same order of magnitude, and in the sequel we do not distinguish between the two.

C. The effect of the polymer at large *k*-vectors

In this section and the following one, we discuss the effect of the B_n field on the u_n field for k vectors much larger and much smaller than k_c. We will show that the spectrum $\langle |u_n|^2 \rangle$ exhibits essentially the same scaling exponent as the Sabra model, but the *amplitude* is affected by the presence of the B_n field. This will be an important factor in the mechanism of drag reduction. Begin with k_n large, $k_n \gg k_c$. In this regime, the effect of the relaxation time τ on the dynamics of the B_n field is completely negligible. The dynamics of B_n is dominated by its coupling to u_n, simply because $u_n k_n \gg \tau^{-1}$. But then in this regime the dynamics is like the one of MHD, which had been analyzed in detail in Ref. [14]. The

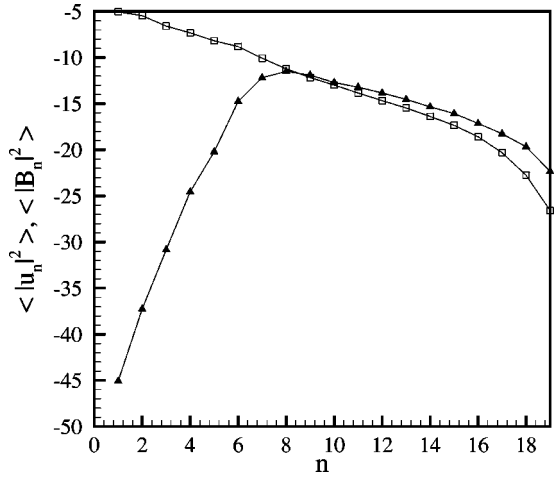

FIG. 10. Double logarithmic plot (to base 2) of the energy spectrum of the Sabra-P model (continuous line with squares). The line with black triangles represents the energy spectrum of the *B* field.

central conclusion of that analysis is that up to intermittency corrections, the spectra of both B_n and u_n fields exhibit a scaling exponent $\zeta_2=2/3$. Indeed, inspecting Fig. 10, we see that for large k_n the two spectra have similar slopes, although intermittency affects the two spectra in different ways.

On the other hand, the amplitudes of the two spectra need not be the same. The relative displacement of the two power laws is determined by numerical details in the model. To estimate this displacement we will estimate the amplitudes of the two spectra at the dissipative scale. The contribution to the dissipation of u is mainly from the small scales, i.e., very large values of k_n. We can define an effective scale k_d, the scale at which energy dissipation peaks:

$$\sum k_n^2\langle|u_n|^2\rangle \sim k_d^2\langle|u_d|^2\rangle, \tag{28}$$

where $u_d=u(k_d)$ and k_d is of the order of the Kolmogorov scale. Since we found that the dissipative scale hardly changes when we add the coupling to the B_n field, we can deduce from Eq. (20) that

$$\langle|u_d|^2\rangle_{SP}-\langle|u_d|^2\rangle_S \approx \sum_n \frac{\langle|B_n|^2\rangle}{\nu\tau}. \tag{29}$$

On the other hand, the sum on the RHS of Eq. (29) is a geometric sum dominated by the contribution of $B(k_c)$, where B_n is maximal. We thus estimate the relative displacement of the two spectra at high values of k_n by

$$\langle|u_d|^2\rangle_{SP}-\langle|u_d|^2\rangle_S \approx \frac{\langle|B(k_c)|^2\rangle}{\nu\tau}. \tag{30}$$

Thus to the first approximation, we expect the slopes of the two spectra to remain unchanged, maintained at a constant difference from each other as given by Eq. (30), until k_n approaches k_c from above, where the effect of the relaxation time τ on the dynamics of B_n cannot be neglected.

D. The effect of the polymer at small *k* vectors

Next, we discuss the slope of the u_n spectrum for $k_n \ll k_c$. This is very easy, since the amplitude of B_n is very small due to the very efficient exponential damping by τ. Thus, the u_n field hardly experiences the coupling to B_n, and its slope, up to intermittency corrections, is again of the order of $\zeta_2=2/3$. Again, the amplitude is changed compared to the pure Sabra case, and this is the most important feature that is discussed next.

E. The tilt in the spectrum at $k_n \approx k_c$

Considering the spectrum in Fig. 10 we note that the B_n spectrum increases rapidly when $k_n \to k_c$ from the left. To understand this phenomenon consider the equation of motion for B_n at steady state. To leading order

$$0=\left\langle\left|\frac{dB_n}{dt}\right|\right\rangle \sim \langle|c_1 k_n u_{n+1}^* B_{n+2}|\rangle - \frac{\langle|B_n|\rangle}{\tau}, \tag{31}$$

where we have neglected terms of the order of B_{n+1}, but including them will lead to similar conclusions. Using the fact that $|k_{n+1}u_{n+1}^*\tau| \ll 1$, and since $|k_{n+1}u_{n+1}^*B_{n+2}| \leqslant |k_{n+1}u_{n+1}^*||B_{n+2}|$ we immediately conclude that

$$\langle|B_n|\rangle \ll \langle|B_{n+2}|\rangle. \tag{32}$$

We continue this argument recursively to estimate the largest polymer contribution $B(k_c)$ as

$$\langle|B(k_c)|\rangle \sim \frac{\langle|B_0|\rangle}{\langle|k_1u_1|\rangle\langle|k_3u_3|\rangle\cdots\langle|k_{c-1}u_{c-1}|\rangle\tau^{n_c/2}}, \tag{33}$$

where $\lambda^{n_c}=k_c$.

In the vicinity of the scale k_c, we have, to leading order in B, in the kinetic energy equation,

$$0=-k_nS_{n+1}-bk_nS_n+(1+b)k_{n-2}S_{n-1} - k_n\langle u_n^*B_{n+1}^*B_{n+2}\rangle. \tag{34}$$

When the amplitude of the polymer goes to zero ($B_n \to 0\ \forall\ n$) the only solution is the well known scaling law $S_n \propto k_n^{-1}$. However, the last term in Eq. (34) forces now a tilt in the spectrum. Its sign is exactly such that S_{n-1} has to increase compared to S_n and S_{n+1}, respectively. Of course, for $k_n \ll k_c$ the effect of the B_n field on the u spectrum is again negligible and therefore, the spectral slope will settle back to the Sabra value. However if the tilt in the vicinity of k_c results in crossing the Sabra spectrum, we would have a whole spectral range where the energy is higher.

We therefore conclude that the existence of drag reduction depends rather heavily on the sign of the energy transfer at scales close to k_c. To check the sign directly in the numerics and thus to substantiate the existence of the tilt, we return to the equations of motion and write

$$\frac{d}{dt}|u_n|^2=\Psi_1^{(n)}(u,u,u)-\Psi_2^{(n)}(u,B,B)-\nu k_n^2|u_n|^2,$$

$$\frac{d}{dt}|B_n|^2=\Psi_3^{(n)}(u,B,B)+\Psi_2^{(n)}(u,B,B)-\frac{1}{\tau}|B_n|^2, \tag{35}$$

where the term $\Psi_1^{(n)}(u,u,u)$ represents the kinetic energy flux of the field, while $\Psi_2^{(n)}(u,B,B)$ is the energy flux going from the velocity field to the polymer field. Finally, term $\Psi_3^{(n)}(u,B,B)$ is the flux of energy of the polymer field due to the transport of the velocity field. Figure 11 shows $\Psi_1^{(n)}$, $-\Psi_2^{(n)}$, and $\Psi_3^{(n)}$ for $\tau=0.4$ and $\nu=10^6$, the same parameters of Fig. 7. It is important to observe that $\Psi_1^{(n)}$ becomes positive for $n>n_c$. For a given n, the term $\Psi_1^{(n)}$ can be written as $\Psi_1^{(n)}=L_n-S_n$, where L_n is the amount of energy flux given from the large scale to scale k_n and S_n is the amount of energy flux given from scale k_n to smaller scales. It follows that when the energy flux is constant, $L_n=S_n$ and, therefore, $\Psi_1^{(n)}(n)=0$. On the other hand, a positive value of $\Psi_1^{(n)}(n)$ implies that $L_n>S_n$. This is exactly what is shown in Fig. 11. The imbalance of the energy flux $\Psi_1^{(n)}$ is compen-

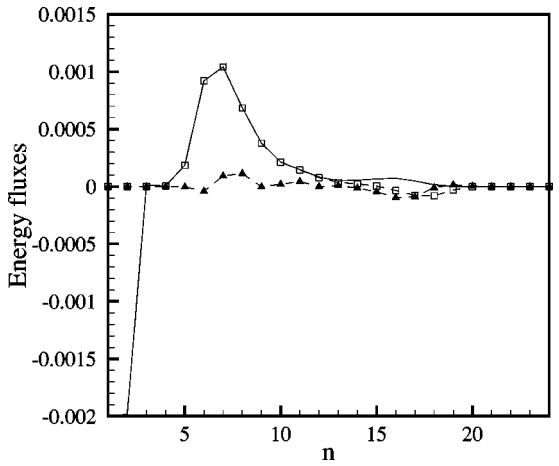

FIG. 11. Energy fluxes for the Sabra-P model. The continuous line corresponds to the fluxes of the kinetic energy $\Psi_1^{(n)}$. The squares correspond to $-\Psi_2^{(n)}$. The dashed line with black triangles is $\Psi_3^{(n)}$.

sated by the flux of energy from u_n to B_n, given by the term $-\Psi_2^{(n)}$. It is interesting to observe that the last term in the balance equation, namely, $\Psi_3^{(n)}$ is rather small, i.e., the effect of an energy cascade of the polymer is rather weak.

F. Discussion

While we have been able so far to describe a convincing scenario for drag reduction, we still should explain the mechanism for the increase of the large scale energy. Since the field B_n is negligible for small n, the average energy flux per unit time at small n must equal the input work per unit time at the largest scales. However, the energy flux does show time and scale fluctuations which could behave differently for the Sabra and Sabra-P models. More specifically, let us consider the quantity G_n defined in Sec. V B. As already discussed, G_n represents the energy flux at scale k_n due to both the nonlinear terms in the velocity field *and* the nonlinear term in the B_n field. In terms of G_n, we can build a large scale energy flux $W_L = G_2 + G_3 + G_4$ which represents the full amount of energy flux across the largest scales, namely, across k vectors $k_n < k_c$, for which the average energy flux is invariant to the changing of Sabra to Sabra-P. The definition of W_L is such that $W_L > 0$ means an energy flux from large scales to small scales. In Fig. 12, we show the probability distribution of W_L for both models, with numerical parameters $\nu = 10^{-5}$ and $\tau = 0.4$. The vertical line in the figure indicates the average value, which, as expected, is invariant. As one can observe, the two probability distributions show a substantial difference for *negative* values of W_L: in the Sabra-P model, one can have larger and more frequent negative values of the energy flux. This can happen even if the instantaneous value of the total energy per unit time obtained by the polymer field from the velocity field is always positive. Qualitatively, this means that while the velocity field is always forcing the polymer field, at very large scales the flux can, from time to time, be reversed, and the polymer field forces the velocity there. This is how the amplitude of the energy spectrum is being increased on an average.

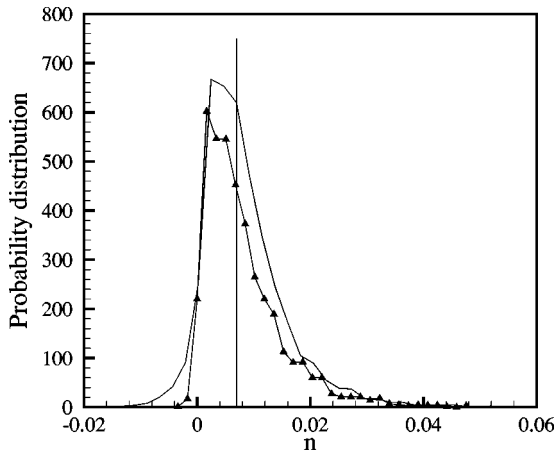

FIG. 12. Probability distribution functions of W_L for the Sabra model the (line with black triangles) and Sabra-P model (continuous line).

Clearly, this mechanism could not work unless the ''forcing'' by the polymer field acted in phase with the growing kinetic energy. In order to clarify this further, we present two time-series of the kinetic energy and W_L, in Fig. 13 for the Sabra model and in Fig. 14 for the Sabra-P model. A close inspection of the figures shows that the reverse of the energy flux W_L occurs exactly during the growing phase of the kinetic energy, leading therefore to a larger value of the instantaneous kinetic energy. This *in phase* mechanism is responsible for drag reduction. Note that this mechanism strongly depends on the large scale dynamics and the value of k_c. For k_n larger than k_c, no significant difference in the statistical behavior of the energy flux is observed. However, the amount of energy forcing, due to the polymer at large scale, can depend on the Reynolds number, at least in the Sabra-P model. If this is the case, then drag reduction should depend on the Reynolds number only through the two relevant scales appearing in the systems, namely, k_c and λ_T, the latter being the Taylor microscale

$$\lambda_T \equiv \sqrt{\frac{E_u}{\sum_n k_n^2 |u_n|^2}}, \tag{36}$$

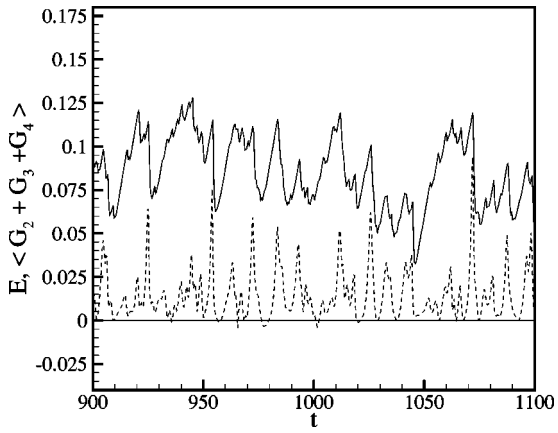

FIG. 13. Time series of the kinetic energy (continuous line) and $2W_L$ (dotted line) for the Sabra model.

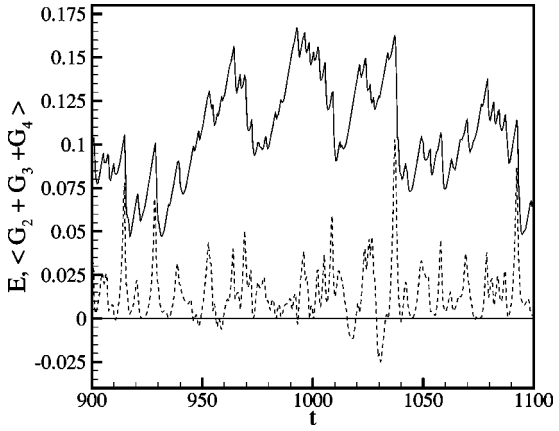

FIG. 14. Time series of the kinetic energy (continuous line) and $2W_L$ (dotted line) for the Sabra-P model.

which also depends on τ in the Sabra-P model. Because the drag is a dimensionless quantity, we argue that the only way in which the Reynolds number may appear in the drag reduction is by means of the dimensionless quantity $\mu = k_c \lambda_T(\tau)$.

There is a simple argument, proposed in the following section, which explains why at large Reynolds numbers one may observe the same qualitative mechanism, i.e. drag reduction, with smaller effects on the kinetic energy. As a matter of fact, the numerical results show that drag reduction reaches its maximum for $\mu \sim 1$

VI. PREDICTIONS OF THE THEORETICAL MECHANISM

We summarize the mechanism of drag reduction using the diagram shown in Fig. 15. The tilt in the spectrum occurs in the vicinity of k_c, with the asymptotic slope for $k_n \ll k_c$ and $k_n \gg k_c$ remaining essentially unchanged. With such a spectrum, the two inequalities (21) and (22) are obviously obeyed.

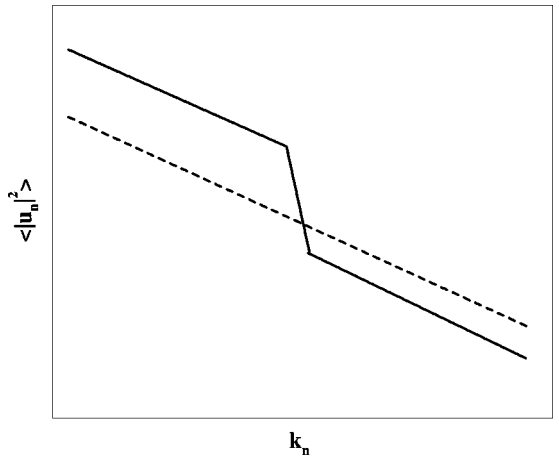

FIG. 15. Double-logarithmic schematic of the effect of polymers in the drag reduction on the turbulence energy spectrum. Dotted line: neat fluid. Solid line: polymeric solution. The spectral slope is unchanged for large and small scales, while at scale k_c there is a significant upward tilt.

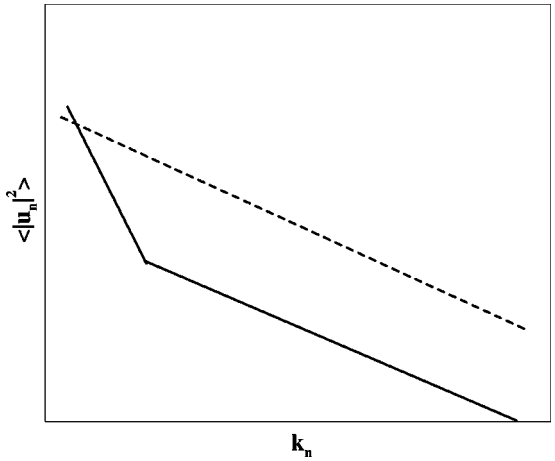

FIG. 16. Double logarithmic schematic of the turbulence energy spectrum when the polymer relaxation time scale is too slow, and the Reynolds number is too large.

The difference in the spectra for $k_n \gg k_c$ is determined predominantly by Eq. (29). This equation predicts that this difference will be greatly increased when the Reynolds number is increased (i.e., when $\nu \to 0$), see Fig. 16. Of course, if this happens we can lose the whole effect of the drag reduction, since the amount of tilt at k_c is basically independent of ν. We need to maintain the spectral difference small enough for the tilt to effect a crossing of the spectrum of Sabra-P and Sabra. Also, the position of k_c is important. If we reduce k_c (i.e., increase τ) the tilt is too far to the left and therefore it will fail to increase the energy. In fact, it can be drag enhancing. The combined effect of decreasing ν and increasing τ is shown in Fig. 16. Needless to say, also if we decrease τ too much we may lose drag reduction since the tilt will be pushed to the irrelevant dissipative range where no energy containing modes exist. Also, if τ becomes too low, B_n becomes smaller, and the amount of tilt is decreased, as can be seen directly from Eq. (34). Although decreasing the field B_n brings the spectra closer together in the large k_n regime, the tilt may not suffice to reduce the drag. Such a situation is shown schematically in Fig. 17. Actually, using the language introduced in the preceding section and the above discus-

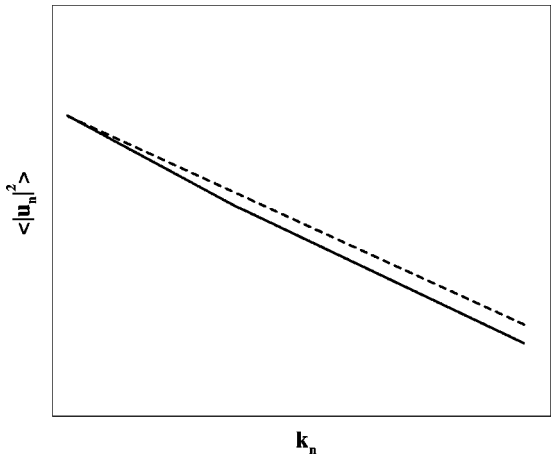

FIG. 17. The relaxation time τ is to low.

sions, we are able to give another argument to understand how drag reduction could depend on the Reynolds number. As previously mentioned, the relevant dimensionless number in the system is $\mu = k_c \lambda_T$. If $\tau \to \infty$ then $k_c \to 0$ and we know that drag reduction must be inhibited. It follows that for $\mu \to 0$ we cannot observe drag reduction. For fixed k_c and increasing Reynolds number, $\lambda_T(\tau)$ decreases as well, although not necessarily as $\mathrm{Re}^{-1/2}$, where Re is the Reynolds number. Then, for fixed τ and increasing Reynolds number we should observe a decreasing effect of drag reduction, as observed in our numerical simulation. The same reasoning can be applied to get information for small Reynolds numbers, as the following argument shows. For $\tau \to 0$ we have already shown that no drag reduction is possible simply because $k_c \to \infty$. This is equivalent to saying that when μ becomes too large there cannot be any drag reduction. It follows that for small Re, i.e., for large λ_T, drag reduction disappears.

VII. CONCLUSIONS AND DISCUSSION

In this paper we discussed several points concerning the possible formulation of a theory for drag reduction in a turbulent flow with a dilute polymer. It is worthwhile, therefore, to review the following main points.

(a) We have introduced a shell model resembling the dynamical properties of the FENE-P equations. Besides any theoretical considerations, the model shows drag reduction in a way close to what is already observed in the numerical simulations of the FENE-P. The implications of this result is that one need not focus on boundary effects or dynamical properties of coherent structure in order to capture the basic physics of drag reduction.

(b) There exists a relevant scale in the system, k_c defined by the so called ''time criterion,'' i.e., $u(k_c)k_c \sim \tau^{-1}$. In the vicinity of this scale, there is a tilt in the spectrum which causes a crossing of the Sabra-P velocity spectrum above the Sabra spectrum for $k_n < k_c$. This in its turn means an increase in the kinetic energy at large scales. Drag reduction can be physically understood in terms of the energy exchanges between the velocity field and the polymer field for $k_n \sim k_c$. We have succeeded in proposing a coherent picture, based on the equation of motions, for the dynamics which is in close agreement with the numerical results.

(c) Drag reduction is a property of large scale flow and its dynamics. This implies that a quantitative description of drag reduction must depend on the details of the flow, the forcing mechanism, as well as the Reynolds numbers. Although a general qualitative mechanism should occur in all drag reduction flows, the amount of drag reduction itself depends on how much energy is *intermittently* given to large scale velocity. Thus, large scale fluctuations are important for a quantitative theory.

(d) Drag reduction by no means could be reduced to the dynamics at the dissipation scale. Although drag reduction could be Reynolds dependent, drag reduction cannot be reduced to a simple increase of the dissipation length. Actually, the dissipation scale does not seem to be affected by drag reduction.

ACKNOWLEDGMENTS

We thank Carlo Casciola, Victor L'vov, and Renzo Piva for many useful discussions. This work has been supported in part by the European Commission under a TMR grant ''Non-ideal Turbulence'' and The Minerva Foundation, Munich, Germany. R.G. thanks the Defence R & D Organisation, Government of India for financial support.

[1] J.L. Lumley, Annu. Rev. Fluid Mech. **1**, 367 (1969).
[2] P.S. Virk, AIChE J. **21**, 625 (1975).
[3] T.S. Luchik and W.G Tiederman, J. Fluid Mech. **190**, 241 (1987).
[4] J.M.J. de Toonder, M.A. Hulsen, G.D.C. Kuiken, and F.T.M. Niewstadt, J. Fluid Mech. **337**, 193 (1997).
[5] R.B. Bird, C.F. Curtiss, R.C. Armstrong, and O. Hassager, *Dynamics of Polymeric Fluids* (Wiley, New York, 1987), Vol. 2.
[6] A.N. Beris and B.J. Edwards, *Thermodynamics of Flowing Systems with Internal Microstructure* (Oxford University Press, New York, 1994).
[7] E. de Angelis, C. Casciola, R. Benzi, and R. Piva (unpublished).
[8] C.D. Dimitropoulos, R. Sureshdumar, and A.N. Beris, J. Non-Newtonian Fluid Mech. **79**, 433 (1998).
[9] E. de Angelis, C.M. Casciola, and R. Piva, Comput. Fluids **31**, 495 (2002).
[10] E. Balkovsky, A. Fouxon, and V. Lebedev, Phys. Rev. E **64**, 056301 (2001).
[11] P.-G. de Gennes, *Introduction to Polymer Dynamics* (Cambridge University Press, Cambridge, 1990)
[12] R. Benzi and I. Procaccia (unpublished); e-print cond-mat/0210523.
[13] P. Giuliani and V. Carbone, Europhys. Lett. **43**, 527 (1998).
[14] E.S.C. Ching, Y. Cohen, T. Gilbert, and I. Procaccia, Phys. Rev. E **67**, 016304 (2003)
[15] V.S. L'vov, E. Podivilov, A. Pomyalov, I. Procaccia, and D. Vandembroucq, Phys. Rev. E **58**, 1811 (1998).
[16] E. de Angelis, C. Casciola, V.S. L'vov, R. Piva, and I. Procaccia (unpublished).
[17] K.R. Sreeinvasan and C.M. White, J. Fluid Mech. **409**, 149 (2000).